Int J Interact Des Manuf (2017) 11:623–632
DOI 10.1007/s12008-016-0336-1

ORIGINAL PAPER

Hydraulic and rotor-dynamic interaction for performance evaluation on a Francis turbine

Manuel Garcia[1] · **Santiago Laín**[2] · **Santiago Orrego**[1,3] · **Jaime Barbosa**[1] · **Brian Quintero**[2]

Received: 10 June 2016 / Accepted: 24 June 2016 / Published online: 29 June 2016

Abstract This paper proposes a new methodology to evaluate the technical state of a Francis turbine installed in a hydroelectric plant by coupling computational fluid dynamics (CFD) and rotor-dynamic analysis. CFD simulations predicted the hydraulic performance of the turbine. The obtained field forces, due to the fluid-structure interaction over the blades of the runner, were used as boundary condition in the shaft rotor-dynamic numerical model, which accurately predicted the dynamic behavior of the turbine's shaft. Both numerical models were validated with in situ experimental measurements. The CFD model was validated measuring the pressure fluctuations near the rotor–stator interaction area and the torque and radial force in the shaft using strain gages. The rotor-dynamic model was validated using accelerometers installed over the bearings supporting the shaft. Results from both numerical models were in agreement with experimental measurements and provided a full diagnose of the dynamic working condition of the principal systems of the turbine. Implementation of this methodology can be applied to further identify potential failure and improve future designs.

Keywords CFD · Fluid structure interaction · Francis turbine · Diagnosis · Vibrations

✉ Manuel Garcia
mgarcia@eafit.edu.co

Santiago Laín
slain@uao.edu.co

Santiago Orrego
sorrego@jhu.edu

Jaime Barbosa
jbarbosa@eafit.edu.co

Brian Quintero
bquinter@uao.edu.co

[1] Departamento de Ingeniería Mecánica, Universidad EAFIT, Medellín, Colombia

[2] Departamento de Energética y Mecánica, Universidad Autónoma de Occidente, Cali, Colombia

[3] Department of Mechanical Engineering, Johns Hopkins University, 3400 N. Charles St, Baltimore, MD, USA

1 Introduction

Francis turbines have been used to produce electrical power for more than a century and their design and performance has evolved during this time. However, several non-desirable unsteady hydraulic phenomena are still present during regular operation including rotor–stator interaction, vortex rope in the draft tube and cavitation. These phenomena propagates along all the components of the machine and are responsible for vibrations, noise and flow instabilities.

Modern diagnosis techniques have been recently applied to estimate the technical state of hydraulic machines by combining the experimental evaluation of the system with computer models [1,6]. Maintenance Based on Models identifies potential failure by establishing relations between the real object and a virtual model [14], extending machines lifetimes, keeping the quality and low cost of operations and preventing the occurrence of system failures [5]. In most cases, machines are in constant operation and studying their dynamic behavior facilitates a better understanding of their working condition or failure detection.

One important technique in diagnosis is vibration analysis. Instruments for measuring vibrations (e.g. accelerometers) can be located strategically around machines and the parameters extracted from the acquired signals are used as effective indicators of the technical state. However, the interpretation of these parameters could be complicated because vibration

is a symptom of a variety of phenomena and their interaction. Francis turbines are complex systems and the safe operation and life of turbines relies on the shaft stability, which can be predicted with rotor-dynamic studies identifying relations between the symptom and its causes of measurements [32,34].

The use of computational fluid dynamics (CFD) in the design and analysis of water turbines started in the late seventies [13] using simplified Quasi-3D Euler solutions and fully 3D potential flow solutions. Over the years the complexity of the approach increased in stages: from 3D Euler solutions, to steady RANS (Reynolds Averaged Navier–Stokes Equations) simulations of single blade passages, extending to steady simulations of whole machines, until today unsteady RANS equations solved in combination with advanced turbulence models [18,19]. CFD of hydraulic machines has become a powerful tool that requires validation with carefully designed and executed experimental measurements. Highly sophisticated and expensive CFD studies are used to understand complex flow mechanisms and multi-physical problems [4] along all the components of the turbine. The most active areas of research and development are now concerned about considering the effects of two-phase flow and fluid-structure interaction [9,13,17,30].

The state of the art, in the three-dimensional flow computation in hydraulic turbomachinery considering the friction and turbulence effects, is solving the Reynolds averaged Navier–Stokes equations (RANS). There is a large number of publications employing this methodology investigating different hydraulic phenomena for different proposes. For example, Ritzinger [25] shows detailed results of turbulent viscous flow in rotors, and Shuliang [29] investigates the pressure drop and the 3D velocity field in a rotor. Schenkel [26] computes the viscous flow in a hydraulic rotor channel assuming rotational symmetry. A common limitation in those numerical simulations is the definition of the boundary conditions between the components of a turbine, which can lead to convergence problems during solution. The coupled calculation of various components (i.e. connecting several components) or a full analysis of the turbomachine facilitates the calculation of the interactions between the elements and alleviate convergence difficulties.

A basic issue in the flow computation through coupled components of the turbine is the modeling of the relative movement between the rotor (moving) and the stator blades (fixed). The two quasi-stationary hypothesis, frozen rotor and mixing plane disregard the terms of temporal evolution in the Navier Stokes equations, therefore, the model does not account for relative motion. Despite neglecting the non-stationary terms, this hypothesis is widely used by many authors, since it has great benefits including saving of computational time when compared to non-stationary methods. Sedlar and Mensik compare both methods for radial [27] and axial pumps [28] and Muggli et al. for a pump-turbine [22]. The investigations by Von Hoyningen-Huene et al. [35] and Chen et al. [3] simulated the rotation of the rotor by averaging several relative positions. The secondary flow in the coupled stationary calculation is investigated in Majidi [20] while Zimnitzki [39] considers the influence of the rotor in the optimization of the spiral case. Nevertheless, employing quasi-stationary hypothesis between rotating and static components of a turbomachinery provides validated solutions with a relatively low computational cost.

The increase in computer power allowed the use of turbulence models in the numerical simulation of turbines. For instance, Treutz used the k-ϵ model [33] and Ojala et al. used the k-ω model [24]. They illustrated the influence of considering the effects of rotation on turbulence model through three variants. However, these produce marginal changes in the velocity field, which are due to the turbulent viscosity change. Ng and Tang recommend using at least two models of turbulence equations for use in turbomachinery [23]. Other works include the use of Large Eddy Simulation (LES) in a Francis turbine and the impeller of a centrifugal pump [2,31].

On the other hand, the mechanical modelling of rotating machinery (e.g. shaft) and their associated support structures (e.g. bearings) has been developed to a high degree of sophistication over the past twenty years, especially by the use of finite element analysis [37]. Accurate models are invaluable in the resolution of a wide variety of rotor-dynamic problems and are often required in connection with computerized monitoring for the detection and diagnosis of faults [38]. However, a limiting factor of current FEM computations is the lack of accurate boundary conditions of the hydraulic force in the runner due to the interaction with the fluid, which is a major contributor to the shaft loading. Using incorrect boundary conditions in rotor-dynamic models incorrectly predicts behavior, specially in hydraulic turbines where the hydraulic phenomena is highly unsteady. Estimating the deformation of the turbine shaft is relevant for diagnosis tasks by determining the severity of the vibrations after spectral decomposition [41].

Karlsson et al. [12] studied the rotor-dynamic behavior of a runner of a hydraulic turbine including loads from the generator and fluid. Results evidenced that unbalance and geometric properties of the turbine and generator are possible sources of the most dominant frequency peak. However, the considered fluid model was based on results from the scientific literature. This paper presents a methodology to estimate the deformation of the shaft of a Francis turbine by coupling a CFD numerical model (i.e. estimation of fluid forces) with a rotor-dynamic numerical model (i.e. estimation of shaft dynamics). This work overcome the limitation of assuming random fluid forces over the shaft. Results present the technical state of the system for a specific operation condition.

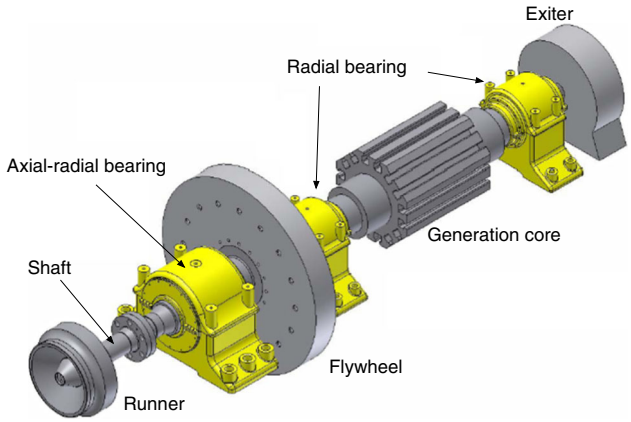

Fig. 1 Schematic view of the turbine components

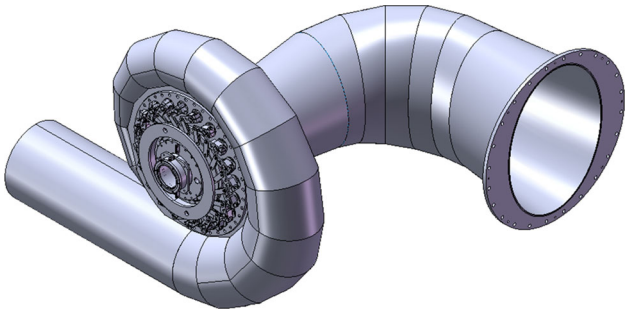

Fig. 2 Turbine geometry considered for the CFD simulations

An interactive response of the CFD and rotordynamics variables in the deformation of the shaft and its vibration is a desire outcome. However, CFD simulations are a computationally intensive process. The results depend upon the quality and size of the mesh. Also, turbulent models add additional degrees of freedom that need to be solved. Interactive fluid simulations were initially relegated to real time visualization [15]. Computational steering, or interactive control over CFD simulations during execution has been a goal during the last years thanks to the increase on computer power. For example it has been tested to simulate interactively indoor climate and to evaluate human comfort [36], and to simulate wind tunnel like environments [8]. Computational steering of complex structures as a Francis turbine is still not possible. The methodology developed here uses an experimentally validated turbine simulation that is coupled with a rotordynamic model and can be used to interactively test variation of the parameters and perform sensitivity analysis with the aim to identify potential failure and improve component design.

1.1 Turbine specifications

The main focus of this research is to understand the unsteady hydraulic and roto-dynamic operation of the Francis turbine at nominal operation point. The technical specifications of the Francis turbine considered in this study are: power 10 MW, head 230 m and rotational speed of 900 rpm, with a discharge at its optimal operation point of 4.8 m^3/s. The assembly of turbine/generator can be seen in Fig. 1. The shaft is supported by three main bearings (i.e. two radial and one axial-radial), and connected to the flywheel, the generator and the runner.

2 CFD methodology

Numerical unsteady simulations have been carried out with the commercial software ANSYS CFX 10®. This code is based on finite volume method and solves the incompressible unsteady Reynolds Averaged Navier–Stokes (URANS) equations in their conservative form. Transient rotor–stator interaction is described by the sliding mesh method. The set of equations is closed with a two-equation turbulence model: The Shear Stress Transport (SST) [21]. The discretization of the equations is made with a second order Backward Euler implicit scheme and a high-resolution advection scheme. The assumed convergence criterion for RMS residuals of velocity, pressure and turbulent variables is 10^{-5}. The time step is 1.8×10^{-4} s and it corresponds to the time that takes the runner to rotate one degree. The total simulation time is that necessary for the runner to turn three times. The objective of the unsteady CFD simulations was to obtain a force field on the surfaces of the runner (blades, hub and shroud). This information was used as boundary condition in the FEM rotor-dynamic model, which determines the displacement of turbine shaft.

The geometry of the turbine's hydraulic components is shown in Fig. 2. For the CFD simulations four computational domains representing the water passages were considered including the spiral case, the stay and guide vanes, the runner and the draft tube. The meshes of the different domains were numerically connected using different interfaces. The GGI, General Grid Interface, was used between the spiral case and the stay vane and the TRS, Transient Rotor–Stator interface, was used between the runner and the guide vanes, and between the runner and the draft tube.

A hexahedral structured mesh was generated for each independent domain using the commercial software ICEM CFD 10.0®. A mesh density study was performed to verify that the solution is independent of the number of elements. For this purpose, different mesh densities were created for each domain. Table 1 summarized the characteristics of the meshes. Torque at the runner was used as variable of reference to perform the mesh independence analysis. Figure 3 shows that the fine mesh, with 1.3 million grid points, provides a solution independent of the size mesh and with significant computational saving.

Table 1 Mesh sizes considered in the grid independency study

Part/# Nodes	Coarse	Fine	Very fine
Spiral case	200	400	750
Stay and guide vanes (20)	270	450	800
Runner (15)	200	350	400
Draft tube	70	100	100
TOTAL	740	1300	2050

Units are thousands of elements

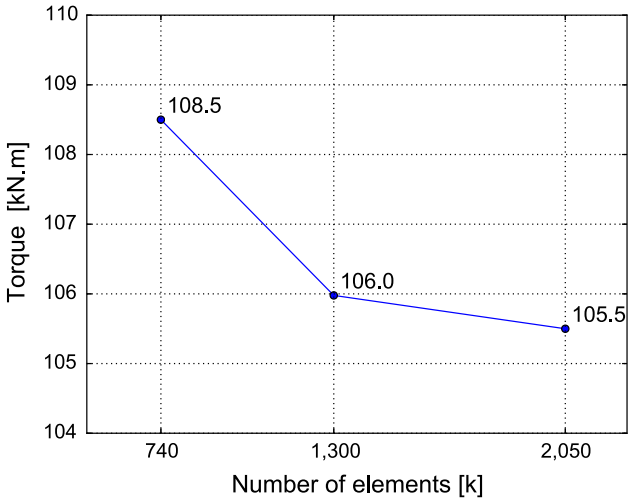

Fig. 3 The mesh independence analysis

Table 2 Boundary conditions used in the unsteady simulation

Boundary condition	Location	Option
Inlet	Spiral case	Mass flow rate
Outlet	Draft tube	Opening
Wall	Solid surfaces	Log Law

A steady-state simulation (RANS) was performed using the same CFD domains and the results were used as the initial conditions for the unsteady simulations. The connection interface between the runner with the guide vanes and the runner with the draft tube was a Frozen Rotor interface considering the relative position of the runner. Figure 4 shows an image of the CFD domain hexahedral meshes.

The boundary conditions used in the steady and unsteady simulations are summarized in Table 2, and represented the conditions at nominal operation point of the turbine.

Results from a CFD simulation provided velocity and pressure values for the entire volume of a domain. In particular the pressure distribution at the runner surfaces represented the hydrodynamic forces extending to the turbine structure. Figure 5 shows the pressure map at the nominal operational condition corresponding to the power of 10 MW. During the simulations, monitoring points were created using the

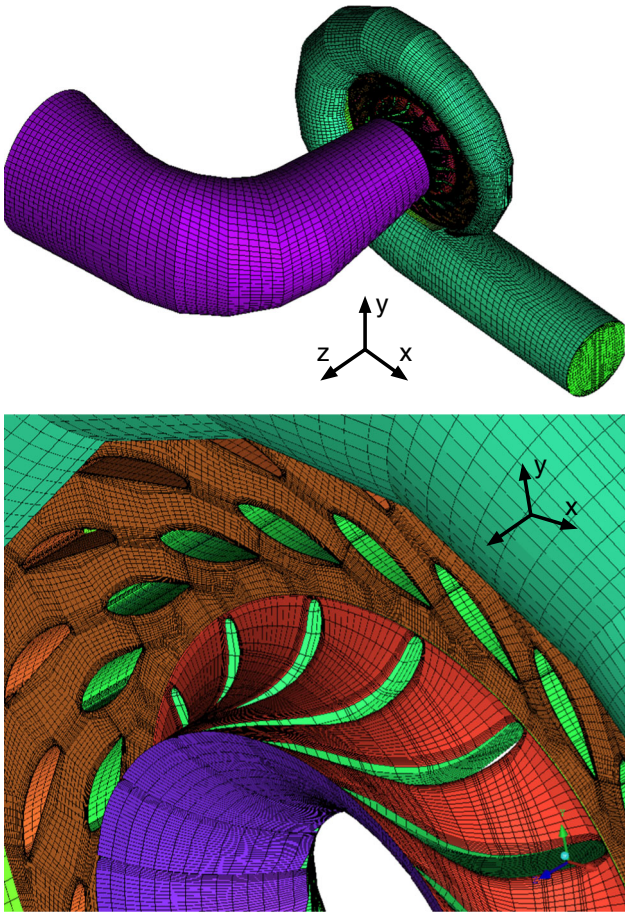

Fig. 4 CFD domain meshes. Close-up view into the stay and guide vanes, and runner

pressure variable as reference, in the same spatial locations where the pressure sensors for experimental measurements were installed. This procedure was performed as a measure of quality control and convergence criteria.

3 Experimental measurements

The experimental validation of the CFD numerical model was accomplished by in situ measurements along different components of the Francis turbine including the draft tube, the spiral chamber, the back cover, the pressure pipe, the shaft and the moving blades. The variables measured at these sections were fluid pressure, acceleration (mechanical vibration), torque and radial force at the shaft. Three dynamic pressure sensors were installed near the zone where the rotor–stator interaction occurs [7,10] and in the draft tube [4]. Figure 6 shows an image of the approximate position of one sensor located at the rotor–stator interaction zone. The color-map in the image corresponds to iso-pressure values obtained by the fluid simulation. The objective of these

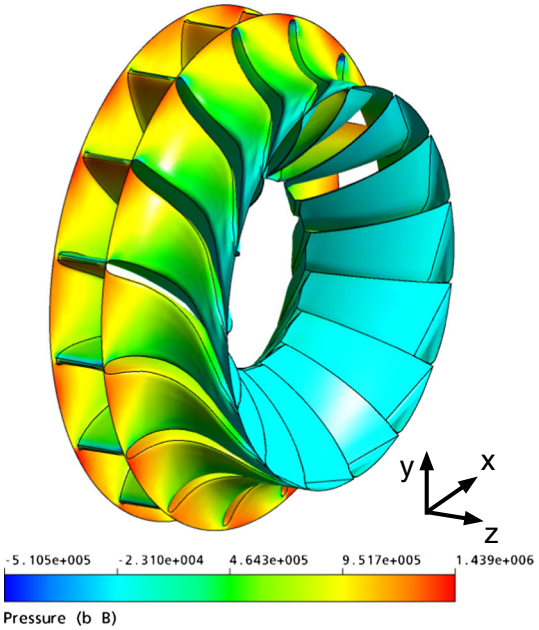

Fig. 5 Pressure distribution in the runner obtained by the simulation at a power of 10 MW. Pressure values at minimum Cp in a range from −0.051 to 1.439 MPa

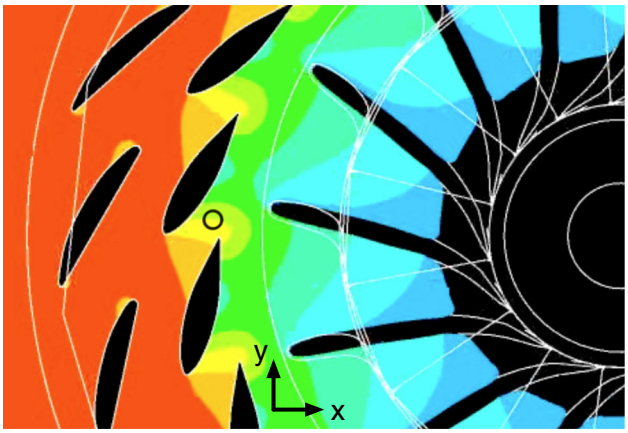

Fig. 6 Pressure sensors are located between guide vanes capturing the effect of rotor–stator interaction. The *colours* correspond to pressure values

measurements was to capture the pressure fluctuations (i.e. rotor–stator interactions) due to the runner blades (rotor) passing near the guide vanes (stator).

Pressure fluctuations at two cross sections of the draft tube were also measured as shown in Fig. 7. The objective of these pressure measurements was to capture vortex rope formation at off-design working conditions of the turbine.

The measurements of the dynamic pressure sensors were recorded performing a simultaneous sampling with 3 s duration. The sampling frequency was 102 kHz capturing more than 40 runner revolutions and more than 6500 samples per channel. This configuration allowed observation of the

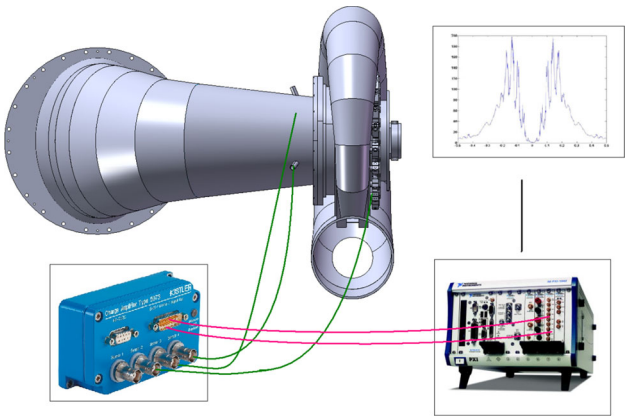

Fig. 7 Setup and distribution of the pressure sensors in the draft tube

hydraulic phenomena (i.e. rotor–stator interaction, vortex rope) appearing at low and high frequencies of the spectrum. Also, strain gages were bonded into the shaft of the turbine to estimate the torque and the radial force on the runner. The measurement setup did not affect the turbine operation in any way as the signals were recorded via wireless connection into the data acquisition equipment. Data collected from the strain gages measurements and dynamic pressure sensors were used to validate the CFD simulations.

3.1 Experimental validation of the simulations

At the spatial points where the dynamic pressure sensors were installed, pressure fluctuations were computed by the unsteady CFD simulation. The numerical simulations calculated the absolute value of the pressure while the experimental measurements only recorded the change of the pressure value. In order to compare both pressure fluctuations signals, the data must be transformed to a non-dimensional reference value called the pressure coefficient C_P, defined as [40]:

$$C_P = \frac{P - \bar{P}}{\frac{1}{2}\rho U^2} \tag{1}$$

where P is the pressure, $\bar{P}$ is the average pressure, ρ is the density and U is the tangential runner velocity.

Figure 8 shows the comparison of pressure fluctuations (C_P) between the experimental (blue) measurements and CFD numerical model (green). The sample length corresponds to 0.07 s, equivalent to 1 rotation of the runner. These signals refer to the sensor placed between the guide vanes and runner. Satisfactory agreement between both signals (numerical and experimental) can be observed.

According to Zobeiri et al. [40], the hydraulic phenomena can be observed in the frequency domain including rotor–stator interaction and vortex rope. The frequency of

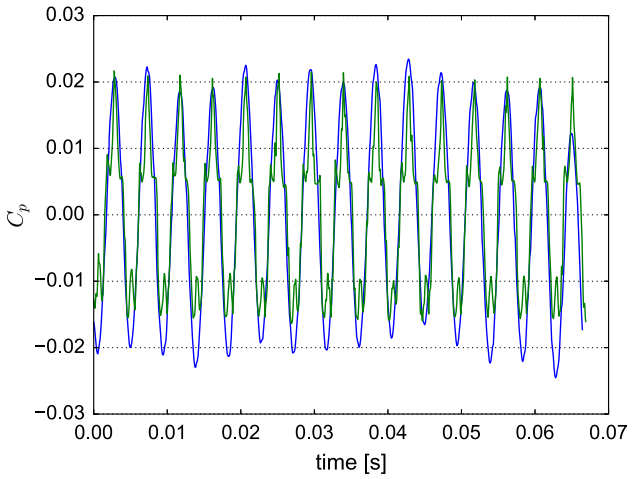

Fig. 8 C_P vs. time at best efficiency point. Numerical (*green*) and experimental (*blue*) data (colour figure online)

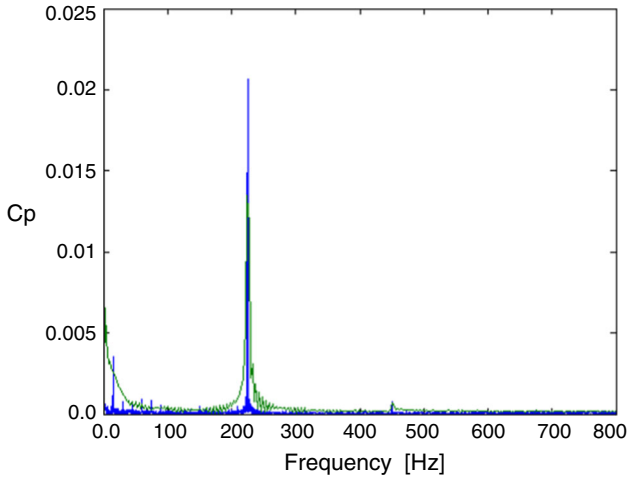

Fig. 9 Power spectrum at best efficiency point. Numerical (*green*) and experimental (*blue*) data (colour figure online)

the rotor–stator interaction is defined by $f_b = N_b f_r$, where N_b is the number of runner blades and f_r is the rotation frequency. For the turbine of this study $f_b = 225$ Hz. The numerical and experimental signals were transformed using Fast Fourier Transform (FFT). Figure 9 shows the power spectrum of both signals clearly representing the rotor–stator interaction hydraulic phenomena at 225 Hz. In addition there is a satisfactory agreement between the numerical and experimental signals, despite discrepancies in amplitude.

Additional validation between the CFD model and experimental measurements was performed comparing the power, torque and radial force as presented in Table 3. Details of the CFD approach to the problem are presented in Lain et al. [18]. The power and torque error was less than 1 % for this operational condition. On the other hand, the radial force, required by the rotor-dynamic numerical model showed a 5 % error. Therefore, this validation process indicates that the CFD model adequately represents the hydraulic behavior of the turbine.

Table 3 Validation of CFD model

	Power (MW)	Torque (kN m)	Max. radial (kN)
Experimental data	9993	105.47	21.92
CFD data	9987	105.52	22.88
Error (%)	0.06	0.05	4.39

4 Rotor-dynamic analysis

A rotor-dynamic numerical model was developed to study the behavior of the shaft of the Francis turbine using the software MESWIR® developed by the Institute of Fluid Flow Machinery (IFM) from the Polish Academy of Science. This code is based on the discretization of the shaft by sections and has three modules for the full system analysis: two modules solve the static and dynamic behavior of the shaft and the third module solves the behavior of the oil film of each bearing.

The rotor-dynamic simulation considered a turbine shaft with different elements attached along the axis direction (runner, flywheel, generator and main exciter), and it was supported by three hydrodynamic bearings fixed in a foundation, see Fig. 1. The external forces acting on the shaft were hydraulic forces resulting from the fluid-runner interaction, magnetic pull resulting from the rotor–stator eccentricity of the generator, unbalanced masses and inertia of the masses of the attached elements. These forces generated vibrations on the system, which were reflected in a series of orbits of the shaft displacement in the bearings (x) [14]. The displacements in the shaft were given by the following non-linear differential equations:

$$M\ddot{x} + D(x, \dot{x})\dot{x} + K(x, \dot{x})x = P(t), \tag{2}$$

where M is the global mass matrix of the system, D the global damping matrix, K the global stiffness matrix and $P(t)$ is the external load or excitation. The required boundary conditions were the support conditions, the forces or external excitations and the mechanical and geometrical properties of the shaft.

The shaft was supported by three hydrodynamic bearings and were represented in the model by their corresponding stiffness and damping coefficients. The determination of those parameters required additional computation of the fluid mechanics. The bearings were attached to a foundation represented by springs and dampers, whose coefficients must be determined separately by previous experiments and numerical computations. Erosion and misalignment conditions were not considered in this model.

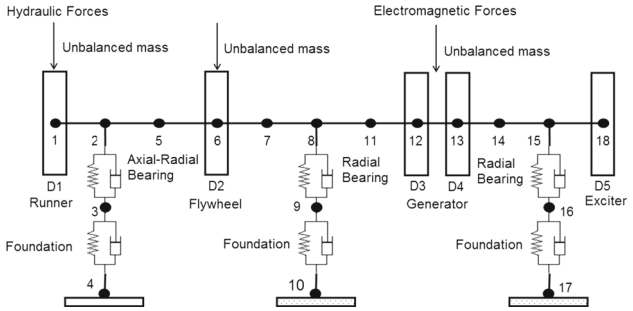

Fig. 10 Simplified diagram of the mechanical model for the shaft supported by three bearings

Equation (2) is a nonlinear equation, as matrices D and K generally depend on the displacements and velocities. Therefore an iterative process is required for its solution. At each step of this process, the coefficients of stiffness and damping of the oil film of the hydrodynamic bearing were estimated because these values depend on the movement parameters of the shaft. This is the main cause of nonlinearity of the system in the present configuration.

The computational model of the shaft was represented in a simplified way as presented in Fig. 10. In this figure, nodes 3–4, 9–10 and 16–17 represent the supporting structure; nodes 3, 9, and 16 represent the hydrodynamic bearing nuts; and nodes 2–3, 8–9, and 15–16 represent the oil film of the hydrodynamic bearings. The connecting elements are considered as beam elements and D1 to D5 are the rigid discs attached to the shaft representing the runner (D1), flywheel (D2), generator (D3, D4) and exciter (D5).

Numerically, the shaft was discretized in cylindrical elements with different diameters connected through their nodes. In addition, rigid disks were connected to the nodes representing the masses of the runner, the inertia wheel, the generator's rotor and the main exciter. Elements that included the stiffness and damping bearings' properties were also connected to the nodes. The beam elements used for the discretization of the shaft were Timoshenko type with six degrees of freedom, three displacements and three rotations.

The shaft was made from alloyed steel with a density of 7800 kg/m^3, a Young's modulus of 200 GPa and a Poisson's ratio of 0.35. The damping coefficients, representing the shaft energy dissipation, were estimated using the Rayleigh equation, obtaining the values of 1.96/s and 5.09×10^{-5} s.

In order to estimate the support conditions, it was necessary to determine the stiffness and damping coefficients of the structure at the bearings gripping points. These parameters were found by performing a computational modal analysis of the foundation with finite elements. The results of the computational analysis were validated with experimental measurements of the structure vibration during the operation. This allowed finding modal parameters in the vibration signals recorded during the operation. As a result, the stiffness and damping coefficients of nodes 3, 9 and 16 of Fig. 10 were obtained following the methods described in [16]. Moreover, the oil film in the hydrodynamic bearings were subjected to a hydrodynamic pressure distribution induced by the rotation of the shaft, which originated a reaction force. Such pressure distribution was described by the Reynolds equation of lubrication theory, which was solved numerically (using a finite difference method) under the hypothesis of laminar flow and constant viscosity along the thickness of the lubricating film. From the pressure distribution, the resulting force was calculated providing the stiffness and damping coefficients as the derivatives of the resulting force with respect displacements and displacement velocities, respectively [42]. Such coefficients were applied in the nodes 2, 8 and 15 of Fig. 10.

Table 4 Mass and inertias of elements attached to the shaft

Element	Runner D1	Flywheel D2	Generator D3, D4	Exciter D5
Mass (kg)	673	8806	9977	500
Inertia (kg m^2)	73	6372	4634	68

Static forces acting on the shaft were considered. The weight of each element attached to the shaft was represented as rigid disks in the model and assumed to be fabricated with steel. Such discs added mass and inertia to the system but they did not represent additional stiffness or damping. Table 4 shows such values.

Dynamic forces acting on the shaft were represented by harmonic excitations having different origins including inertial, hydraulic and magnetic. The hydraulic forces were generated by the fluid-structure interaction in the runner and were determined with CFD simulations previously described in Sect. 2. Magnetic forces arose as a consequence of the rotor eccentricity with respect to the generator stator; this caused asymmetric distribution of the magnetic flux and an unbalance force in the direction of the smallest air gap. The magnetic pull was estimated by following the analytic procedure shown in [11], providing in this case a value of 4966 N. Finally, inertial forces were unknown a priori and they were an output of the numerical computation that allowed tuning the model to experimental measurements on the real technical object. This force was included as unbalanced masses placed at certain radius in specific locations. For this case they were located on the runner, flywheel and generator, i.e. at nodes 1, 6 and 12–13 of Fig. 10.

The mechanical model of the shaft was evaluated numerically in the software MESWIR®, which is based in the finite element method. Static as well as dynamic analyses were performed. Figure 11 presents a scheme showing how the different numerical methods were coupled to solve the mechanical model of the shaft.

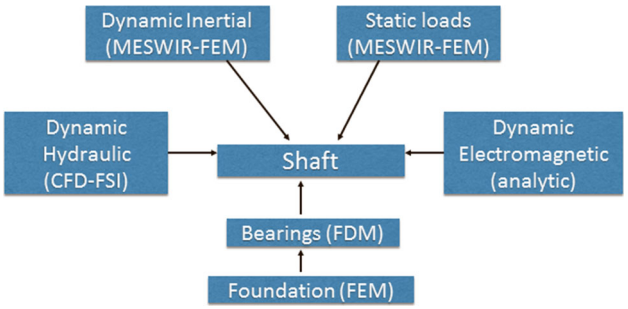

Fig. 11 Scheme of numerical methods employed in the shaft model

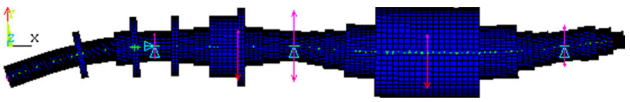

Fig. 12 Deformed shaft (deformation scale 1000:1)

4.1 Results of rotor-dynamic analysis

Initially, the shaft was subjected to a series of deflections attributed to its own weight and to the static loads applied, which moved its axis with respect to the supporting points. These deflections were estimated through static computation. As an example, the deformed shaft is illustrated in Fig. 12, where the triangles represent the supporting points.

In this case, the maximum deformation appears in the runner and it was computed by the software as 188 μm. To study the vibration dynamics of the shaft, the effect of dynamic forces were taken into account as harmonic forces, acting at the rotational frequency of the machine (equal to 15 Hz), introduced as unbalanced masses at specific unbalanced radii. This method was used because the shaft unbalance gives rise to vibrations with the frequency equal to that of the rotation. The dynamic module of MESWIR allowed predicting the vibration ellipses of the shaft in the supporting points. Figure 13, shows the numerical vibration amplitudes of the shaft (continuous line) compared with the experiments (small circles) at the three bearings.

As presented in Fig. 13, the non-linear dynamic module of the software provided fairly good agreement with the experiments regarding the vibration displacements on the supporting points. For this case, the unbalanced conditions, which are an output of the software, are shown in Table 5. In addition, it can be noticed that the values for the displacement are below the limit value, $A < A_{\text{lim}} = 165\,\mu\text{m}$, where A_{lim} is the limit of relative journal-bush vibrations, expressed by the p-p dislocation amplitude in two directions at an angle of 45° with respect to the perpendicular, and given by the ISO 7919-2 standard for relative vibration. Although not shown, it was also verified that VRMS $<$ VRMS$_{\text{lim}} = 7.5$ mm/s, where VRMS$_{\text{lim}}$ is the limit of absolute bearing vibrations, expressed by RMS vibration velocities in the horizontal and vertical directions, which is given by the ISO 10816-2 standard for absolute vibration.

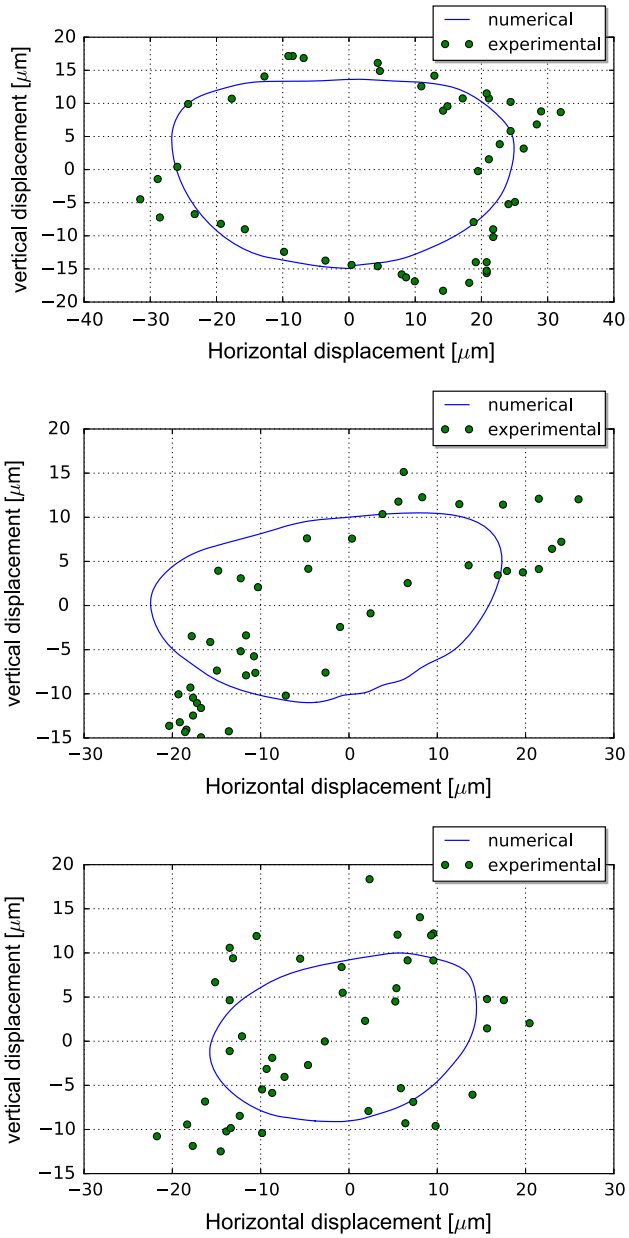

Fig. 13 Vibration amplitudes in the shaft at the three supporting points. Bearing 1 (*top*), bearing 2 (*middle*) and bearing 3 (*bottom*)

Table 5 Unbalance conditions (mass and radii) for the shaft elements

Type of force	Unbalanced mass (kg)	Unbalanced radius (m)
Hydraulic	0.113	0.5
Electromagnetic	0.226	0.5
Unbalanced runner	2.650	0.5
Unbalanced flywheel	7.000	0.5
Unbalanced generator	6.000	0.5

There are some limitations in this investigation. Effects such as erosion of the elements in contact with the fluid and

misalignment at the connectors of the shaft with the system can modify the geometry and therefore the stiffness, inertia and damping matrices. It is also possible to overcome the unbalance of the system by, for instance, following the procedure stipulated by the 1940 ISO standard.

5 Conclusions

Numerical and in situ experimental investigations were conducted to evaluate the technical state of a Francis turbine installed in a power plant. Unsteady CFD simulations successfully predicted the hydraulic behavior of the turbine and reproduced correctly the frequencies of the rotor–stator interaction in the machine (225 Hz). In situ experimental measurements validated the numerical results comparing variables such as runner torque and radial force, power and pressure fluctuations near the rotor–stator interaction region showing a satisfactory agreement. The dynamic hydraulic forces over runner surfaces were extracted and used as boundary condition in a rotor-dynamic numerical model using MESWIR. The mechanical model of the shaft predicted lateral vibration displacements, which agreed with in situ measurements over the turbine bearings. For the studied operating condition, the unbalanced masses required are relatively large, which is likely because the rotor is very rigid and significant amounts of residual unbalance could be compatible with acceptable vibration amplitudes. Overall, the presented methodology demonstrated the reliability of performing numerical simulations to determine the technical state of an operating Francis turbine. Once the rotor-dynamic model is experimentally validated, the model can be used to interactively test variation of the parameters and perform sensitivity analysis. This is useful to identify potential failure and improve component design.

Acknowledgements The authors gratefully acknowledge the support received from the EAFIT University, Empresas Públicas de Medellin (EPM), EPFL–LMH Lausanne (Switzerland), the Alberta University (Canada), the Universidad Autónoma de Occidente and COLCIENCIAS under contract 272-11122006.

References

1. Bently, D.E., Hatch, C.T.: Fundamentals of Rotating Machinery Diagnostics. Amer Society of Mechanical (2002)
2. Byskov, R.K., Jacobsen, C.B., Pedersen, N.: Flow in a centrifugal pump impeller at design and off-design conditions. Part II: large eddy simulations, ASME. J. Fluids Eng. **125**(1), 73–83 (2003). doi:10.1115/1.1524585
3. Chen, S.H., Liaw, L.F.: The flowfield calculations of a centrifugal pump with volute. In: International Gas Turbine and Aeroengine Congress and Exhibition, Orlando (1997)
4. Ciocan, G.D., Iliescu, M.S., Vu, T.C., Nennemann, B., Avellan, F.: Experimental study and numerical simulation of the flindt draft tube rotating vortex. J. Fluids Eng. **129**(2), 146–158 (2007)
5. Cui, L.: Maintenance Models and Optimization, pp. 789–805. Springer London (2008). doi:10.1007/978-1-84800-131-2_48
6. Estévez, E.E., do Nascimento, L.d.P., Ferrando, M.d.C.V., Santacreu, E.J.: El diagnóstico de daños en grupos hidroeléctricos mediante el análisis de vibraciones. Ingeniería del agua **1**(3) (1994)
7. Gagnon, J., Deschenes, C.: Numerical Simulation of a Rotor–Stator Unsteady Interaction in a Propeller Turbine. CFD Society of Canada, Toronto (2007)
8. García, M., Duque, J., Boulanger, P., Figueroa, P.: Computational steering of cfd simulations using a grid computing environment. Int. J. Interact. Design Manuf. (IJIDeM) **9**(3), 235–245 (2015). doi:10.1007/s12008-014-0236-1
9. Göz, M., Laín, S., Sommerfeld, M.: Study of the numerical instabilities in lagrangian tracking of bubbles and particles in two-phase flow. Comput. Chem. Eng. **28**(12), 2727–2733 (2004)
10. Guedes, A., Kueny, J.L., Ciocan, G.D., Avellan, F.: Unsteady rotor–stator analysis of hydraulic pump-turbine: CFD and experimental approach. In: 21st IAHR Symposium on Hydraulic Machinery and Systems (2002)
11. Gustavsson, R.: Modelling and analysis of hydropower generator rotors. Lulea University of Technology. The Polhem Laboratory. Division of Computer Aided Design (2005)
12. Karlsson, M., Aidanpää, J.O.: Dynamic behaviour in a hydro power rotor system due to the influence of generator shape and fluid dynamics. In: ASME 2005 Power Conference, pp. 905–913. American Society of Mechanical Engineers (2005)
13. Keck, H., Sick, M.: Thirty years of numerical flow simulation in hydraulic turbomachines. Acta Mech. **201**(1–4), 211–229 (2008)
14. Kicinski, J.: Rotor Dynamics. Wydaw, IMP PAN Gdansk (2006)
15. Kreylos, O., Tesdall, A., Hamann, B., Hunter, J., Joy, K.: Interactive visualization and steering of CFD simulations. In: Proceedings of the symposium on Data Visualisation 2002, pp. 25–34. Eurographics Association (2002)
16. Krodkiewski, A.J.: Dynamics of Rotors. The University of Melbourne (2007). http://www.ktdw.pl/ksiazki/13lec.pdf
17. Laı n, S., Aliod, R.: Study on the eulerian dispersed phase equations in non-uniform turbulent two-phase flows: discussion and comparison with experiments. Int. J. Heat Fluid Flow **21**(3), 374–380 (2000)
18. Laín, S., García, M., Avellan, F., Quintero, B., Orrego, S.: Simulación numérica de turbinas Francis. Fondo Editorial EAFIT (2011). http://www.eafit.edu.co/cultura-eafit/fondo-editorial/colecciones/Paginas/simulacion-numerica-turbinas-francis.aspx
19. López, O., Meneses, D., Quintero, B., Laín, S.: Computational study of transient flow around darrieus type cross flow water turbines. J. Renew. Sustain. Energy **8**(1), 014,501 (2016)
20. Majidi, K.: Numerische berechnung der sekundärströmung in radialen kreiselpumpen zur feststoffförderung. Ph.D. thesis, TU Berlin. Berlin (1997)
21. Menter, F.R.: Two-equation eddy-viscosity turbulence models for engineering applications. AIAA J. **32**(8), 1598–1605 (1994)
22. Muggli, F.A., Eisele, K., Zhang, Z., Casey, M.V.: Numerical investigations of the flow in a pump turbine in pump mode. In: 3rd European Conference on Turbomachinery, pp. 997–1002, Londres (1999)
23. Ng, E.Y.K., Tan, S.T.: Evaluation of turbulence models for fluid machinery application. In: ASME/ JSME Conference. ASME, San Francisco (1999)
24. Ojala, J., Rautaheimo, P., Siikonen, T.: Numerical Simulation of a Centrifugal Pump Using k-Omega Model Including the Effects of Rotation. Wiley, New York (1998)
25. Ritzinger, S.: Simulation realer Laufradströmungen. Herbert Utz Verlag, Munich (1998)

26. Schenkel, S.: Modellierung und numerische simulation der strömungsvoränge am laufradeintritt von turboarbeitsmaschinen. Ph.D. thesis, TU Darmstadt (1998)
27. Sedlar, M., Mensik, P.: Investigation of rotor–stator interaction influence on flow fields in radial pump flows. In: 3rd European Conference on Turbomachinery, pp. 1017–1025, Londres (1999)
28. Sedlar, M., Vlach, M., Soukal, J.: Numerical and experimental investigation of flow in axial flow hydraulic machinery. In: 3rd European Conference on Turbomachinery, pp. 1007–1016, Londres (1999)
29. Shuliang, C.: Three-dimensional turbulent flow in a centrifugal pump impeller under desing and off-desing operating conditions. In: ASME Fluids Engineering Division Summer Meeting (FEDSM99-6872). ASME (1999)
30. Sommerfeld, M., Lain, S.: Parameters influencing dilute-phase pneumatic conveying through pipe systems: a computational study by the euler/lagrange approach. Can. J. Chem. Eng. **93**(1), 1–17 (2015)
31. Song, C.C.S., Chen, X., Ikohagi, T., Sato, J., Sinmei, K., Tani, K.: Simulation of flow through Francis turbine by LES method. In: Proceedings of the 18th Symposium on Hydraulic Machinery and Cavitation, pp. 267–276, Valencia (1996)
32. Stolarski, T.: Turbomachinery Rotordynamics (1995)
33. Treutz, G.: Numerische simulation der instationären strömung in einer kreiselpumpe, Ph.D. thesis. TU Darmstadt, Alemania (2002)
34. Vance, J.M.: Rotordynamics of Turbomachinery. Wiley, New York (1988)
35. Von Hoyningen-Huene, M., Hermeler, J.: Comparison of three approaches to model stator–rotor interaction in turbine front stage of an industrial gas turbine. In: 3rd European Conference on Turbomachinery, pp. 307–322, Londres (1999)
36. Wenisch, P., Treeck, Cv, Borrmann, A., Rank, E., Wenisch, O.: Computational steering on distributed systems: indoor comfort simulations as a case study of interactive cfd on supercomputers. Int. J. Parallel Emerg. Distrib. Syst. **22**(4), 275–291 (2007)
37. Wu, Y., Li, S., Liu, S., Dou, H.S., Qian, Z.: Vibration of Hydraulic Machinery, chap. Rotordynamic Simulation of Hydraulic Machinery, pp. 307–373. Springer Netherlands, Dordrecht (2013).doi:10.1007/978-94-007-6422-4_9
38. Xia, Y., Qiu, Z., Friswell, M.I.: The time response of structures with bounded parameters and interval initial conditions. J. Sound Vibr. **329**(3), 353–365 (2010)
39. Zimnitzki, A.: Beitrag zur optimalen gestaltung des spiralgehäuses einer kreiselpumpe. Ph.D. thesis. TU Dresden, Alemania (2000)
40. Zobeiri, A., Kueny, J.L., Farhat, M., Avellan, F.: Pump-turbine rotor-stator interactions in generating mode: pressure fluctuation in distributor channel. In: 23rd IAHR Symposium on Hydraulic Machinery and Systems, LMH-CONF-2006-008 (2006)
41. Żółtowski, B., Cempel, C.: Engineering of machine diagnostics (2004)
42. Żółtowski, B., Perez, J.L.B., Heredia, L.F.C.: Study of the technical state of a francis turbine by rotor dynamic simulations. Journal of Polish CIMAC **4**(3), 113–123 (2009)